SUPPORTING INFORMATION

Targeting orthosteric and allosteric pockets of aromatase via dual-mode novel azole inhibitors

Jessica Caciolla,[§,a] Angelo Spinello,[§,b] Silvia Martini,[c] Alessandra Bisi,[a] Nadia Zaffaroni,[c] Silvia Gobbi,[a,*] and Alessandra Magistrato[b,*]

a) Department of Pharmacy and Biotechnology, Alma Mater Studiorum-University of Bologna, via Belmeloro 6, 40126, Bologna, Italy.

b) CNR-IOM Democritos c/o International School for Advanced Studies (SISSA), Via Bonomea 265, Trieste, Italy.

c) Fondazione IRCSS Istituto Nazionale dei Tumori, via Amadeo 42, 20113, Milano, Italy.

Supporting Information Content

Figure S1 to S5 Pag. 2-6

Table S1 Pag. 7

Supporting materials and methods Pag. 8-13

References Pag. 14

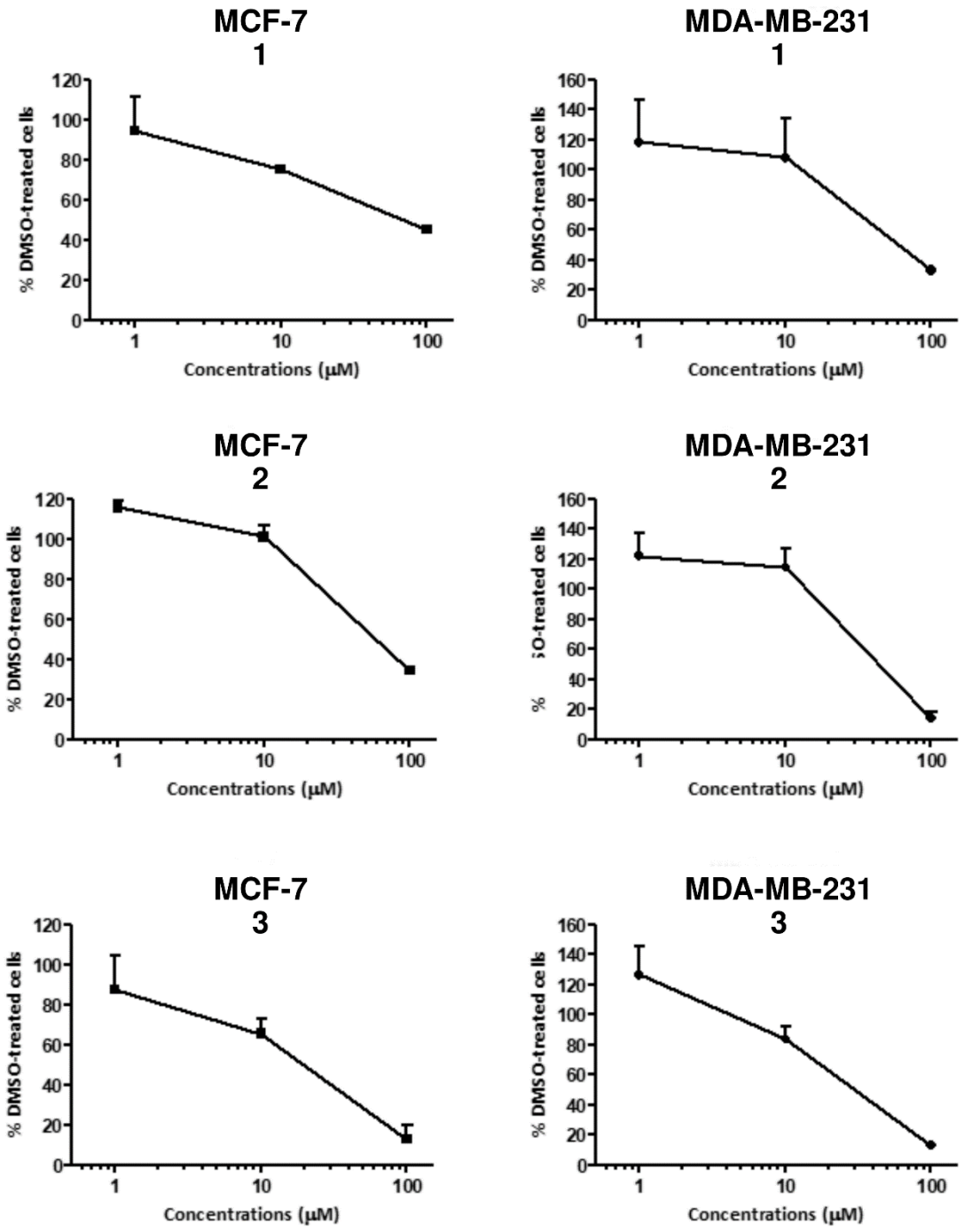

Figure S1: Cellular proliferation assay of compounds **1-3** on ER+ MCF-7 and ER- MDA-MB-231. Cells were cultured for 72 hrs in the presence of increasing concentrations of compounds (1-100 µM). Data are expressed as mean values ± SD of three independent experiments.

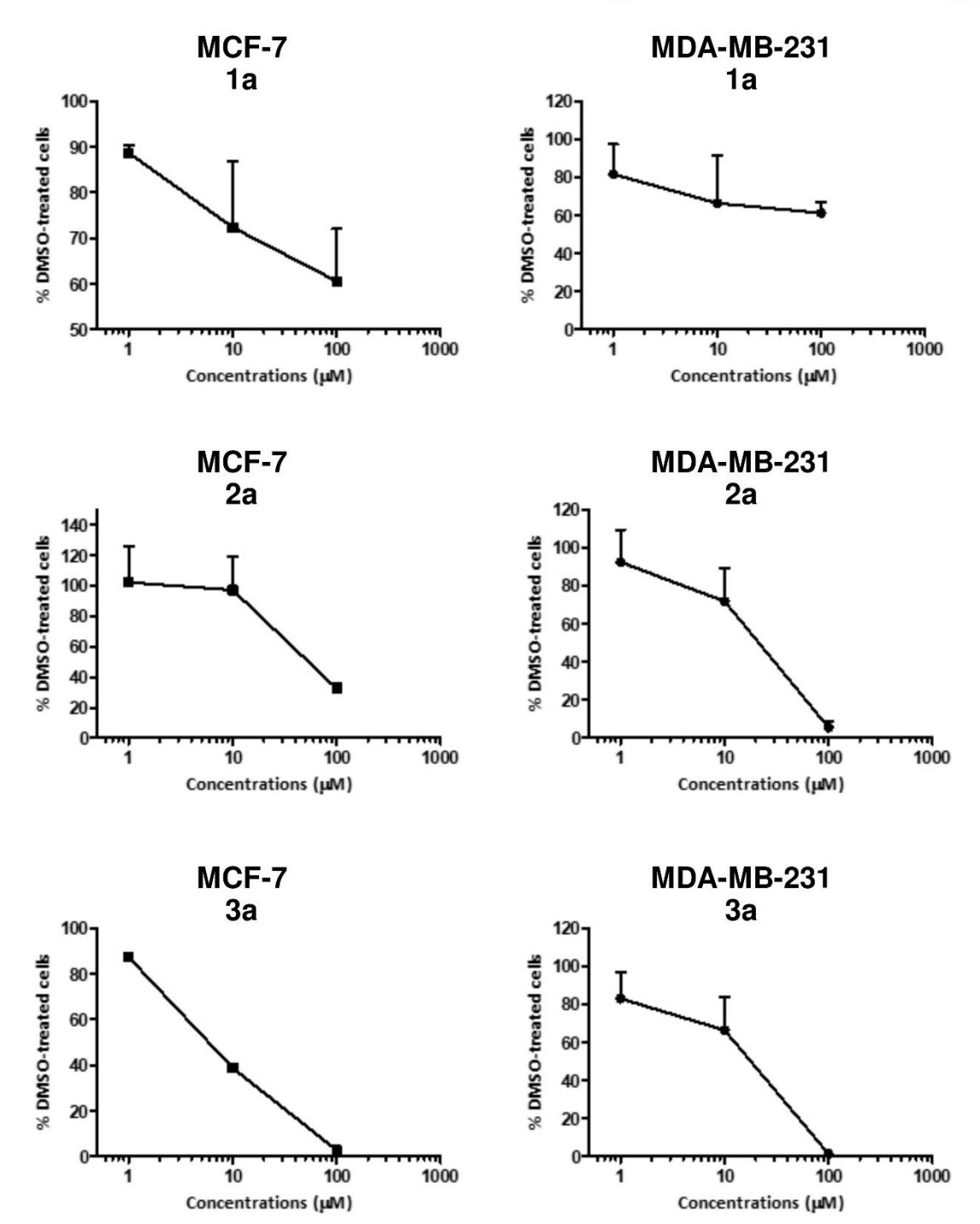

Figure S2: Cellular proliferation assay of compounds **1a-3a** on ER+ MCF-7 and ER- MDA-MB-231. Cells were cultured for 72 hrs in the presence of increasing concentrations of compounds (1-100 µM). Data are expressed as mean values ± SD of three independent experiments.

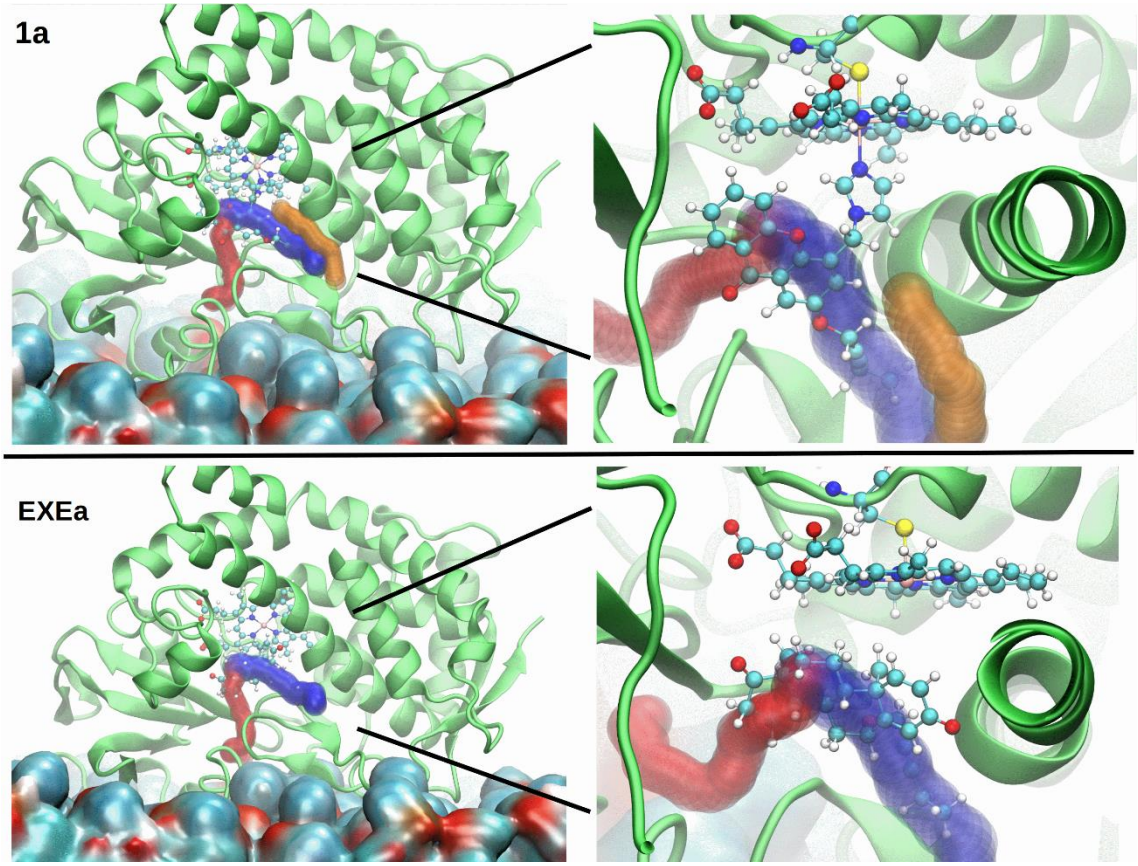

Figure S3: Access/egress channels to/from the catalytic site of the apo form of aromatase enzyme are shown in a Surf representation in red (**ChI**) and blue (**ChII**), respectively[1] and superposed to the binding poses of **1a** and **EXEa**. The steroidal inhibitor EXEa fits perfectly into the pocket, using its pentynyloxy side chain to close **ChII**. In contrast, compound **1a** is not able to perfectly fill **ChII** and a new channel (orange) is detected using Caver webserver.[2] The protein is displayed as green new cartoon, the inhibitor and the heme moiety are shown in a ball and stick representation.

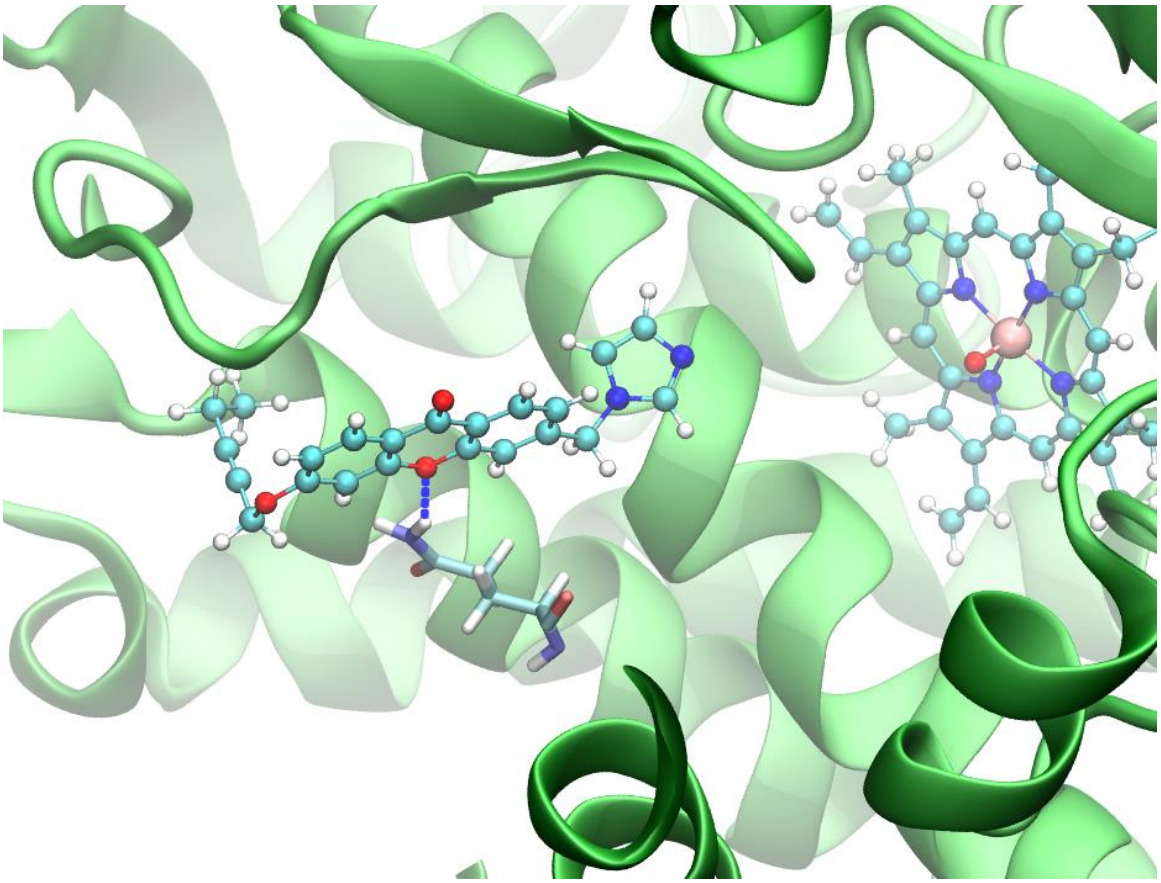

Figure S4: Binding pose of compound **3a** inside the aromatase (HA) access channel (Site 1) as obtained from docking calculations. The protein is displayed as green new cartoon, the inhibitor and the heme moiety are shown in a ball and stick representation, while hydrogen bonds are shown as dashed red and blue lines.

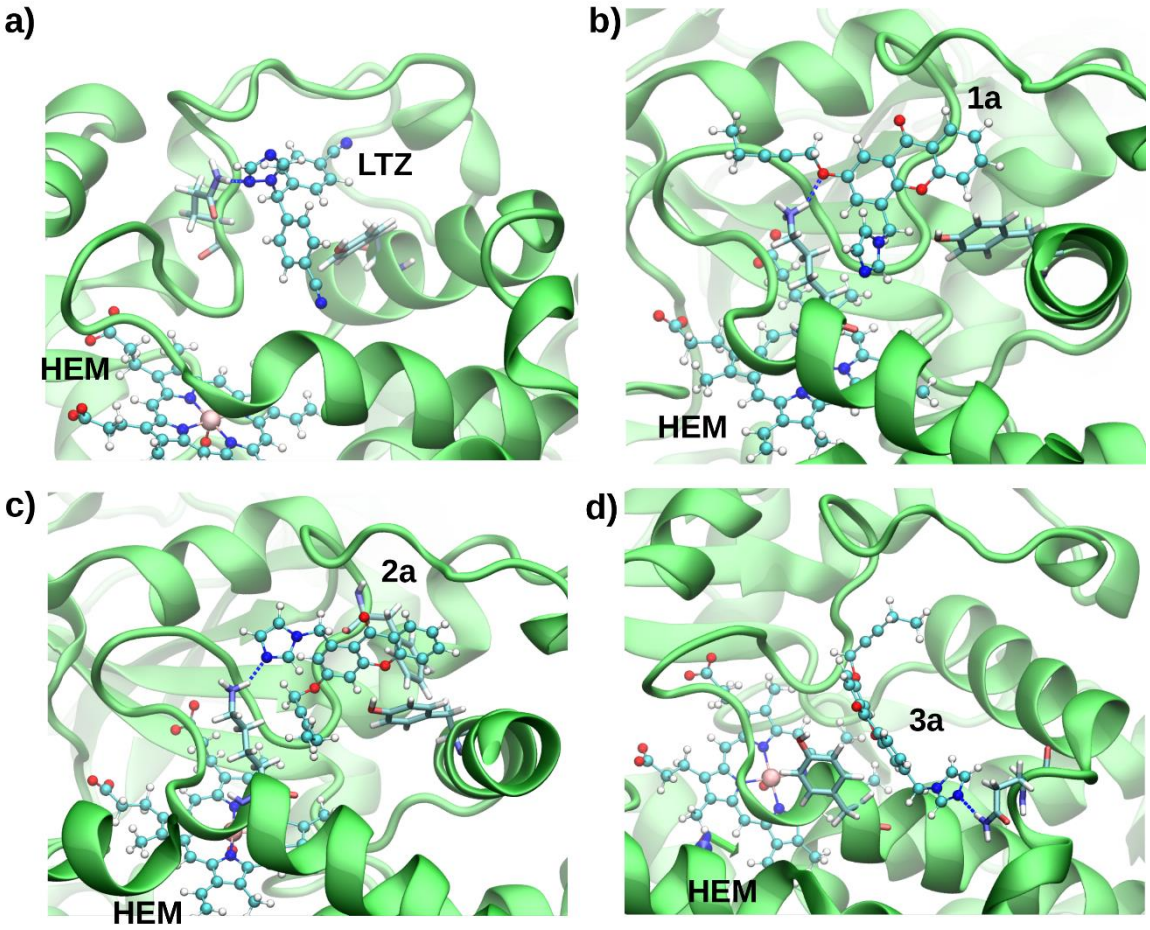

Figure S5: Representative structures as obtained from the docking calculations of letrozole (LTZ)[3] and **1a**-**3a** inside the heme proximal cavity (Site 2). The protein is displayed as green new cartoon, the inhibitors and the heme moiety are shown in a ball and stick representation, the hydrophobic residues involved in stacking and hydrophobic interactions are highlighted as sticks. Hydrogen bonds are represented as dashed blue lines.

Table S1. Potential off-target interactions of the xanthone derivatives. The name of the enzymes are reported along with their ChEMBL IDs[4] and UniProt access codes.[5]

Name	ChEMBL ID	UniProt Accessions
Solute carrier organic anion transporter family member 1B1	CHEMBL1697668	Q9Y6L6
Solute carrier organic anion transporter family member 1B3	CHEMBL1743121	Q9NPD5
Caspase-7	CHEMBL3468	P55210
Alpha-galactosidase A	CHEMBL2524	P06280
Caspase-1	CHEMBL4801	P29466
Monoamine oxidase A	CHEMBL1951	P21397
Beta-glucocerebrosidase	CHEMBL2179	P04062
Endoplasmic reticulum-associated amyloid beta-peptide-binding protein	CHEMBL4159	Q99714
15-hydroxyprostaglandin dehydrogenase [NAD+]	CHEMBL1293255	P15428
Cytochrome P450 3A4	CHEMBL340	P08684
Survival motor neuron protein	CHEMBL1293232	Q16637
Lysine-specific demethylase 4D-like	CHEMBL1293226	B2RXH2
Aldehyde dehydrogenase 1A1	CHEMBL3577	P00352
Microtubule-associated protein tau	CHEMBL1293224	P10636

Supporting materials and methods

Chemistry. General Methods

All chemicals were purchased from Aldrich Chemistry, Milan (Italy), or from Alfa Aesar, Milan (Italy), and were of the highest purity. Melting points were determined in open glass capillaries using a Büchi apparatus and are uncorrected. ^{1}H NMR and ^{13}C NMR spectra were recorded in $CDCl_3$, unless otherwise indicated, on a Varian VXR Gemini spectrometer 400 MHz and 101 MHz, respectively. Chemical shifts are reported in parts per million (ppm) relative to tetramethylsilane (TMS) as internal standard and spin multiplicities are given as s (singlet), d (doublet), t (triplet), m (multiplet) or br (broad). Direct infusion ES-MS spectra were recorded on a Waters Micromass ZQ 4000 apparatus. Chromatographic separations were performed by flash column chromatography on silica gel columns (Kieselgel 40, 0.040-0.063 mm; Merck). Organic solutions were dried over anhydrous sodium sulfate. The purity of the tested compounds was determined by HPLC analysis, performed on a Jasco LC 1500 PU-1587; column: Phenomenex Luna C18(2) 5 μm 4.60 mm × 150 mm; elution conditions: mobile phase CH_3CN/H_2O + KH_2PO_4 0.2 % 50/50; flow-rate: 1 ml/min; injection volume: 20 μl; peaks were detected at 220 nm and results were > 95% purity. Compounds were named relying on the naming algorithm developed by CambridgeSoft Corporation and used in ChemDraw Professional 15.0.

General method for the synthesis of xanthones (4, 7).

A mixture of 2-chlorobenzoic acid (1,0 eq), catalytic amounts of Cu and CuI, K_2CO_3 (2,0 eq), pyridine (0.5 eq) and the selected phenol (1,0 eq) in H_2O was refluxed for 2 h. The basic reaction mixture was then washed with ethylether and acidified with HCl to give a precipitate that was filtered, dried and added portionwise, without further purification, to polyphosphoric acid (PPA, 10:1 w/w). The mixture was heated at 120 °C for 7 h, then poured in ice, the precipitated solid was filtered, suspended in $NaHCO_3$ saturated solution and then filtered again to obtain a crude product that was purified by flash chromatography when needed.

2-methoxy-4-methyl-9*H*-xanthen-9-one (4). Starting from 2-chlorobenzoic acid (1.32 g, 8.44 mmol) and 4-methoxy-2-methylphenol (2.32 g, 16.88 mmol), **4** was obtained (yield 20 %), mp 164-167 °C. ^{1}H NMR: δ 2.57 (s, 3H, CH_3), 3.92 (s, 3H, OCH_3), 7.21 (s, 1H, arom), 7.37-7.41 (m, 1H, arom), 7.53-7.59 (m, 2H, arom), 7.72-7.75 (m, 1H, arom), 8.37 (d, *J* = 7.2 Hz, 1H, arom).

3-methoxy-1-methyl-9*H*-xanthen-9-one (7). Starting from 2-chlorobenzoic acid (2.64 g, 17 mmol) and 3-methoxy-5-methylphenol (4.69 g, 34 mmol), a crude was obtained that was purified by flash column chromatography (petroleum ether/ethyl acetate 4:1) to give **7** (yield 12 %), mp 120-124 °C. ^{1}H NMR: δ 2.91 (s, 3H, CH_3), 3.92 (s, 3H, OCH_3), 6.71 (s, 1H, arom), 6.78 (s, 1H, arom), 7.33-7.37 (m, 1H, arom), 7.41 (d, *J* = 8.4 Hz, 1H, arom), 7.64-7.68 (m, 1H, arom), 8.29 (d, *J* = 9.2 Hz, 1H, arom).

General method for the synthesis of imidazole derivatives (5, 8).

A mixture of the selected methylxanthenone **4** or **7** (1.0 eq), *N*-bromosuccinimide (NBS, 1.0 eq) and a catalytic amount of benzoyl peroxide (BPO) in CCl_4 was refluxed for 6 h. The mixture was hot filtered and evaporated to dryness. The obtained residue, without further purification, was dissolved in acetonitrile and imidazole (3.0 eq) was added. The mixture was refluxed for 6 h under nitrogen, the solvent was evaporated and the residue was purified by flash column chromatography with a suitable eluent.

4-((1*H*-imidazol-1-yl)methyl)-2-methoxy-9*H*-xanthen-9-one (5). Starting from **4** (0.40 g, 1.70 mmol), a crude was obtained that was purified by flash column chromatography (petroleum ether/ethyl acetate 4:1, ethyl acetate) to give **5** (yield 40 %), mp 186-188 °C. ^{1}H NMR: δ 3.90 (s, 3H, OCH_3), 5.51 (s, 2H, CH_2imi), 7.05 (s, 1H, arom), 7.09 (d, *J* = 3.2 Hz, 1H, arom), 7.16 (s, 1H, arom), 7.40-7.44 (m, 1H, arom), 7.51 (d, *J* = 8.0 Hz, 1H, arom), 7.72 (d, *J* = 3.2 Hz, 1H, arom), 7.74-7.78 (m, 1H, arom), 7.95 (s, 1H, arom), 8.35 (dd, *J* = 7.8 e 1.4 Hz, 1H, arom).

1-((1*H*-imidazol-1-yl)methyl)-3-methoxy-9*H*-xanthen-9-one (8). Starting from **7** (0.54 g, 2.25 mmol), a crude was obtained that was purified by flash chromatography (toluene/ethyl acetate 9.75:0.25, then ethyl acetate) to give **8** (yield 84 %), mp 209-210 °C. ^{1}H NMR: δ 3.85 (s, 3H, OCH_3), 5.94 (s, 2H, CH_2imi), 6.20 (s, 1H, arom), 6.85 (s, 1H, arom), 7.02 (s, 1H, arom), 7.15 (s, 1H, arom), 7.37-7.40 (m, 1H, arom), 7.44 (d, *J* = 8.4 Hz, 1H, arom), 7.64-7.73 (m, 2H, arom), 8.28 (d, *J* = 8.4 Hz, 1H, arom).

General method for the synthesis of hydroxyl derivatives (6, 9, 11).

A mixture of methoxyxanthone **5, 8,** or **10** (1.0 eq) and $AlCl_3$ (4.5 eq) in toluene was refluxed for 3 h and evaporated to dryness. Ice was added to the residue and the mixture was allowed to reach room temperature, the precipitate was collected by filtration and purified by flash column chromatography when needed.

4-((1*H*-imidazol-1-yl)methyl)-2-hydroxy-9*H*-xanthen-9-one (6). Starting from **5** (0.23 g, 0.75 mmol) a crude was obtained that was purified by flash chromatography (DCM/methanol 9.5:0.5) to give **6** (yield 69 %), mp 240-242 °C. ^{1}H NMR (methanol-*d*$_4$): δ 5.75 (s, 2H, CH_2imi), 7.02 (s,1H, arom), 7.04 (s, 1H, arom), 7.31 (s, 1H, arom), 7.44 (s, 1H, arom), 7.50-7.52 (m, 1H, arom), 7.64-7.65 (m, 1H, arom), 7.87-7.88 (m, 1H, arom), 8.25 (d, *J* = 8.0 Hz, 1H, arom), 8.89 (s, 1H, arom), 9.41 (s, 1H, OH).

1-((1*H*-imidazol-1-yl)methyl)-3-hydroxy-9*H*-xanthen-9-one (9). Starting from **8** (0.59 g, 1.9 mmol) **9** was obtained (yield 42 %), mp 195-198 °C. ^{1}H NMR (methanol-*d*$_4$): δ 6.00 (s, 2H, CH_2imi), 6.60 (s, 1H, arom), 6.92 (d, *J* = 2.4 Hz, 1H, arom), 7.30 (s, 1H, arom), 7.39-7.43 (m, 2H, arom), 7.52 (d, *J* = 8 Hz, 1H, arom), 7.76-7.80 (m, 1H, arom), 8.20 (dd, *J* = 7.8 and 2,0 Hz, 1H, arom), 8.49 (s, 1H, arom).

3-((1*H*-imidazol-1-yl)methyl)-6-hydroxy-9*H*-xanthen-9-one (11). Starting from **10** [6] (0.57 g, 1.90 mmol) **11** was obtained (yield 68 %), mp 234-236 °C. ^{1}H NMR (methanol-*d*$_4$): δ 5.56 (s, 2H, CH_2imi), 6.87 (s, 1H, arom), 6.92 (dd, *J* = 8.6 and 2 Hz, 1H, arom), 7.35 (d, *J* = 8.4 Hz, 1H, arom), 7.40 (s, 1H, arom), 7.48-7.51 (m, 2H, arom), 8.12 (d, *J* = 8.4 Hz, 1H, arom), 8.27 (d, *J* = 8.0 Hz, 1H, arom), 8.60 (s, 1H, arom).

General method for the synthesis of pentynyloxy final compounds 1a-3a.

A mixture of hydroxyxanthone **6**, **9** or **11** (1.0 eq), K_2CO_3 (1.0 eq) and 1-bromo-2-pentyne (1.0 eq) in acetone was refluxed for 18-26 h (monitored by TLC). The mixture was hot filtered and evaporated to dryness to obtain a residue that was purified by flash chromatography (ethyl acetate/methanol 9.5:0.5).

4-((1*H*-imidazol-1-yl)methyl)-2-(pent-2-yn-1-yloxy)-9*H*-xanthen-9-one (1a). Starting from **6** (0.10 g, 0.34 mmol) **1a** was obtained (yield 18 %), mp 138-140 °C. ^{1}H NMR (acetone-d_6): δ 1.08 (t, *J* = 7.4 Hz, 3H, CH_3), 2.22 (q, *J* = 7.4 Hz, 2H, CH_2), 4.86 (s, 2H, OCH_2), 5.65 (s, 2H, CH_2imi), 6.96 (s, 1H, arom), 7.28 (s, 1H, arom), 7.29 (s, 1H, arom), 7.47-7.51 (m, 1H, arom), 7.73-7.75 (m, 1H, arom), 7.77 (s, 1H, arom), 7.87-7.91 (m, 2H, arom), 8.26 (dd, *J* = 7.8 and 1.4 Hz, 1H, arom). ^{13}C NMR: δ 12.72, 13.96, 45.45, 57.55, 74.85, 90.44, 108.56, 119.10 (2C), 121.90, 123.25, 124.98, 125.18 (2C), 127.01, 129.80, 135.99 (2C), 149.35, 154.83, 156.58, 176.52. MS (ES) *m/z*: 359 (M + H).

1-((1*H*-imidazol-1-yl)methyl)-3-(pent-2-yn-1-yloxy)-9*H*-xanthen-9-one (2a). Starting from **9** (0.23 g, 0.79 mmol) **2a** was obtained (yield 8 %), mp 129-130 °C. ^{1}HNMR: δ 1.15 (t, *J* = 7.6 Hz, 3H, CH_3), 2.25 (q, *J* = 7.6 Hz, 2H, CH_2), 4.71 (s, 2H, OCH_2), 5.94 (s, 2H, CH_2imi), 6.29 (s, 1H, arom), 6.96 (s, 1H, arom), 7.01 (s, 1H, arom), 7.14 (s, 1H, arom), 7.37-7.41 (m, 1H, arom), 7.46 (d, *J* = 8,0 Hz, 1H, arom), 7.64 (s, 1H, arom), 7.69-7.73 (m, 1H, arom), 8.28 (dd, *J* = 7.6 and 1.6 Hz, 1H, arom).^{13}CNMR: δ 12.59, 13.59, 49.91, 57.11, 72.81, 91.12, 101.43, 112.77, 113.20, 117.46, 119.94, 122.57, 124.27, 126.77, 129.83, 134.63, 138.20, 142.27, 155.40, 159.54, 162.54, 177.79. MS (ES) *m/z*: 359 (M + H), 381 (M + Na).

3-((1*H*-imidazol-1-yl)methyl)-6-(pent-2-yn-1-yloxy)-9*H*-xanthen-9-one (3a). Starting from **11** (0.38 g, 1.30 mmol) **3a** was obtained (yield 13 %), mp 118-120 °C. ^{1}H NMR: δ 1.16 (t, *J* = 7.6 Hz, 3H, CH_3), 2.27 (q, *J* =7.6 Hz, 2H, CH_2), 4.80 (s, 2H, OCH_2), 5.30 (s, 2H, CH_2imi), 6.97-7.03 (m, 3H, arom), 7.13 (s, 1H, arom), 7.17-7.19 (m, 2H, arom), 7.64 (s, 1H, arom), 8.26 (d, *J* = 9.2 Hz, 1H, arom), 8.32 (d, *J* = 8.0 Hz, 1H, arom). ^{13}C NMR: δ 12.63, 13.66, 50.39, 57.22, 73.12, 90.99, 101.73, 114.05, 116.00, 116.25, 119.58, 121.81, 122.45, 127.79, 128.44, 130.52, 137.81, 143.41, 156.69, 157.95, 163.54, 175.87. MS (ES) *m/z*: 359 (M + H), 381 (M + Na).

HA inhibition assays

Inhibition of HA was quantified by the Aromatase Inhibitor Screening Kit (BioVision Inc., San Francisco, USA), monitoring the conversion of a fluorogenic substrate into a highly fluorescent metabolite as catalyzed by HA. Namely, after the reconstitution of the reagents, a standard curve was generated by diluting the fluorescent standard. Test compounds were dissolved in DMSO at a final concentration of ≤ 0.25% (v/v), after having verified that such concentration of solvent does not siglificantly affect the HA activity. Each mother solution was diluted in aromatase assay buffer to obtain a range of concentrations for generating a multi-point dose-response curve. The reaction was prepared by adding Aromatase mix (containing Recombinant Human Aromatase (2X), Aromatase assay buffer and NADPH-generating system) to test compounds, inhibitor control, background control and positive control (1 µM LTZ). The reaction mixture was preincubated at 37°C for 10 min to allow test compounds to interact with HA, then, reaction initiated after the

addition of 30 µl of Aromatase Substrate/NADP+ mixture (containing buffer, aromatase substrate and β-$NADP^+$ 100X stock). Assays were done in 96-well microtiter plates (Corning Incorporated, Corning, ME, USA) in a final reaction volume of 100 µl/well. Sample fluorescence was measured using a TECAN Ultra microplate reader (Tecan Trading AG, Switzerland) at dual wavelengths of 488/527 nm for 60 min. Results were expressed as relative fluorescence units (RFUs). Experiments were carried out in triplicate and the average values were used to construct the dose-response curves. The percentage of inhibition was calculated as the ratio between the RFUs of control and test compound, according to the manufacturer's instructions. Tests were done at different concentrations (100, 10, 1 and 0.1 µM). For each compound, the concentration able to inhibit HA activity by 50% (IC_{50}) was calculated by nonlinear regression of the experimental data to a tetraparametric logistic curve (SigmaPlot 13.0 - Systat Software Inc.).

Cell lines and culture conditions

MCF-7 and MDA-MB-231 cell lines were obtained from American Type Culture Collection (ATCC). MDA-MB-231 cells were grown in DMEM-F12 + 5% fetal bovine serum (FBS) and MCF-7 cells in RPMI + 10% FBS. Cells were tested for the absence of *Mycoplasma* fortnightly and maintained in logarithmic growth phase as a monolayer in a humidified 5% CO2 atmosphere at 37°C.

Cell proliferation assays

Cells were seeded in triplicate in 12-well plates (50.000 cells/well and 70.000 cells/well for MDA-MB-231 cells and MCF-7 cells, respectively) and 24 h later exposed for 72 h to increasing concentrations of compounds **1**, **2**, **3**, **1a**, **2a**, and **3a**. Culture medium was then removed and adherent cells were harvested using trypsin and counted with a cell counter (Beckman Coulter, S.p.A., Milan, Italy). All experiments were performed three times. The GI_{50} value was defined as the concentration of a drug inhibiting cell growth by 50%.

Docking calculations

Docking was performed with Glide[7] using the single precision (SP) protocol. A van der Waals (vdW) radius scaling factor of 0.80 Å for protein and ligands atoms having a partial charge less than 0.15 was used to account for protein flexibility. A metal constraint was incorporated in order to obtain binding poses in which the nitrogen atom is coordinated with the heme iron, following a reported procedure.[8] In particular, the ligand nitrogen must be within 2.5 Å of the iron atom to satisfy this constraint. This protocol was, then, validated using the most active imidazolylmethylxanthones compounds, **1-3**, previously reported.[9] After initial failed attempts to obtain a binding pose for compound **3a** and the AI letrozole, an induced fit protocol was employed.[10] In particular, SP docking was performed using a softened vdW radius scaling of 0.50 for ligands and protein atoms possessing a partial atomic charge of 0.15. Afterwards, 100 poses were submitted to Prime[11] to predict new side chains orientations for the residues within a shell of 6 Å from the center of mass of the ligands. Thus, a redocking step was performed for the structures

having score laying within 30 kcal/mol from the best one. All the obtained binding poses were subjected to MD simulations.

Classical MD simulations

An equilibrated model of HA was taken from a previous work.[12] The protonation states under physiological conditions were calculated with the webserver H++.[13] Considering recent literature studies,[14] Asp309 was considered in its neutral form. We have used Parm99SB AMBER FF for the protein,[15,16] Shahrokh *et al.* parameters for the heme moiety and Cys437 [17] and the general Amber FF (GAFF) for the inhibitors.[18] ESP charges[19] were obtained by performing geometry optimization of the structures of the inhibitors at Hartree-Fock level of theory using a 6-31G* basis set with the Gaussian 09 software[20] and were subsequently transformed in RESP charges using the Antechamber module of ambertools 18.[21] Our models were solvated along the x and y direction with TIP3P waters[22] leading to a total of 66342 atoms. Topology, built with ambertools 18, was converted in a GROMACS format using the software acpype.[23] Finally, MD simulations were performed using GROMACS 2018.2,[24] using an integration time step of 2 fs and all covalent bonds involving hydrogen atoms constrained with the LINCS algorithm. Simulations were performed in the NPT ensemble, at a temperature of 300 K, using a velocity-rescaling thermostat.[25] An initial energy minimization step was done with the steepest descend algorithm. A preliminary equilibration of the model was performed for 20 ns with the protein and ligand atoms harmonically restrained using a force constant of 1000 kJ mol^{-1} nm^{-2}. Afterwards, constraints were released, and the model was slowly thermalized to reach the target temperature of 300 K within 10 ns. Then, in order to assess the stability of the docking poses obtained each system was relaxed by performing a 100 ns MD simulation.

QM/MM Molecular Dynamics

QM/MM Born Oppenheimer MD simulations were performed using CP2K 6.1 program.[26-28] The QM layer, including the heme group and the inhibitors (96 atoms), was simulated in a cubic box with sides of 24 Å and it was described at Density Functional Theory (DFT) BLYP[29,30] level using a dual Gaussian-type/Plane Waves basis set (GPW).[26] In particular, we employed a double ζ (MOLOPT) basis set,[31] an auxiliary PW basis set with a density cutoff of 400 Ry and Goedecker-Teter-Hutter (GTH) pseudopotentials.[32,33] This protocol has been used successfully in many QM/MM MD simulations of biomolecules.[34-37] The dangling bonds between the quantum and classical regions were saturated using capping hydrogens atoms. An integration step of 0.5 fs was used in all the QM/MM MD simulations in the NVT ensemble. All systems were initially optimized and equilibrated at 300 K without constraints for 5 ps, using a Nosé-Hoover thermostat,[38] followed by other 5 ps after the stable formation of the coordination bond has occurred. After preliminary benchmarks and consistently with other studies,[39] the heme was simulated with a doublet spin state. For the classical region we have used the same force field of the classical MD simulations.

QM/MM Metadynamics (MTD)

If the formation of the coordination bond between the iron and the nitrogen atoms was not observed during the QM/MM MD equilibration run, metadynamics (MTD) simulations were performed. Representative snapshots obtained from the QM/MM MD trajectories were used as starting points for MTD simulations, using the implementation of the cp2k code. A simple collective variable (CV1) was used to describe the formation of the coordination bond, involving the distance between the two atoms. Gaussian hills with a height of 0.6 kcal/mol and a width of 0.10 Å were added every 15 fs. The simulation was stopped when a minimum in the FES was obtained and the binding poses were further relaxed by 5 ps of QM/MM MD.

Analysis

Cluster analysis and root mean square deviation (RMSD) of the MD trajectories were performed using g_cluster tool, based on the Daura et. al algorithm[40] and g_rmsd as implemented in the GROMACS 2018.2 package. The Amber 18 tool MM_PBSA.py[41] was used to perform Molecular Mechanics Generalized Born Surface Area (MM-GBSA) free energy calculation, taking 100 frames from an equilibrated part of the MD trajectories. An improved generalized born solvation model was employed (igb=8),[42] and a salt concentration of 0.1 M. Visualization of the MD trajectories and images were done using the VMD program.[43] Access/egress channels were analyzed using the Caver webserver.[2] The ChEMBL databases was used to search for possible off-targets of the investigated compounds.[4] We have not found any entries for imidazolylmethylxanthones derivatives with or without a pentynyloxy side chain substituent in any position. Instead, for the xanthone moiety a total number of 14 target enzymes are known.

References:

1. Magistrato, A.; Sgrignani, J.; Krause, R.; Cavalli, A. Single or Multiple Access Channels to the CYP450s Active Site? An Answer from Free Energy Simulations of the Human Aromatase Enzyme. *J. Phys. Chem. Lett.* **2017,** 8, 2036-2042.
2. Stourac, J.; Vavra, O.; Kokkonen, P.; Filipovic, J.; Pinto, G.; Brezovsky, J.; Damborsky, J.; Bednar, D. Caver Web 1.0: identification of tunnels and channels in proteins and analysis of ligand transport. *Nucleic Acids Res.* **2019,** 47, W414-W422.
3. Spinello, A.; Martini, S.; Berti, F.; Pennati, M.; Pavlin, M.; Sgrignani, J.; Grazioso, G.; Colombo, G.; Zaffaroni, N.; Magistrato, A. Rational design of allosteric modulators of the aromatase enzyme: An unprecedented therapeutic strategy to fight breast cancer. *Eur. J. Med. Chem.* **2019,** 168, 253-262.
4. Gaulton, A.; Hersey, A.; Nowotka, M.; Bento, A. P.; Chambers, J.; Mendez, D.; Mutowo, P.; Atkinson, F.; Bellis, L. J.; Cibrian-Uhalte, E.; Davies, M.; Dedman, N.; Karlsson, A.; Magarinos, M. P.; Overington, J. P.; Papadatos, G.; Smit, I.; Leach, A. R. The ChEMBL database in 2017. *Nucleic Acids Res* **2017,** 45, D945-D954.
5. UniProt, C. UniProt: a worldwide hub of protein knowledge. *Nucleic Acids Res* **2019,** 47, D506-D515.
6. Gobbi, S.; Hu, Q.; Zimmer, C.; Belluti, F.; Rampa, A.; Hartmann, R. W.; Bisi, A. Drifting of heme-coordinating group in imidazolylmethylxanthones leading to improved selective inhibition of CYP11B1. *Eur. J. Med. Chem.* **2017,** 139, 60-67.
7. Friesner, R. A.; Banks, J. L.; Murphy, R. B.; Halgren, T. A.; Klicic, J. J.; Mainz, D. T.; Repasky, M. P.; Knoll, E. H.; Shelley, M.; Perry, J. K.; Shaw, D. E.; Francis, P.; Shenkin, P. S. Glide: a new approach for rapid, accurate docking and scoring. 1. Method and assessment of docking accuracy. *J. Med. Chem.* **2004,** 47, 1739-49.
8. Caporuscio, F.; Rastelli, G.; Imbriano, C.; Del Rio, A. Structure-based design of potent aromatase inhibitors by high-throughput docking. *J. Med. Chem.* **2011,** 54, 4006-17.
9. Gobbi, S.; Zimmer, C.; Belluti, F.; Rampa, A.; Hartmann, R. W.; Recanatini, M.; Bisi, A. Novel highly potent and selective nonsteroidal aromatase inhibitors: synthesis, biological evaluation and structure-activity relationships investigation. *J. Med. Chem.* **2010,** 53, 5347-51.
10. Sherman, W.; Day, T.; Jacobson, M. P.; Friesner, R. A.; Farid, R. Novel procedure for modeling ligand/receptor induced fit effects. *J. Med. Chem.* **2006,** 49, 534-53.
11. *Small-Molecule Drug Discovery Suite 2017-1*, Schrodinger, LLC: New York, 2017.
12. Sgrignani, J.; Magistrato, A. Influence of the membrane lipophilic environment on the structure and on the substrate access/egress routes of the human aromatase enzyme. A computational study. *J. Chem. Inf. Model.* **2012,** 52, 1595-606.
13. Anandakrishnan, R.; Aguilar, B.; Onufriev, A. V. H++ 3.0: automating pK prediction and the preparation of biomolecular structures for atomistic molecular modeling and simulations. *Nucleic Acids Res.* **2012,** 40, W537-41.
14. Di Nardo, G.; Breitner, M.; Bandino, A.; Ghosh, D.; Jennings, G. K.; Hackett, J. C.; Gilardi, G. Evidence for an elevated aspartate pK(a) in the active site of human aromatase. *J. Biol. Chem.* **2015,** 290, 1186-96.
15. Wickstrom, L.; Okur, A.; Simmerling, C. Evaluating the performance of the ff99SB force field based on NMR scalar coupling data. *Biophys. J.* **2009,** 97, 853-6.
16. Lindorff-Larsen, K.; Piana, S.; Palmo, K.; Maragakis, P.; Klepeis, J. L.; Dror, R. O.; Shaw, D. E. Improved side-chain torsion potentials for the Amber ff99SB protein force field. *Proteins* **2010,** 78, 1950-8.
17. Shahrokh, K.; Orendt, A.; Yost, G. S.; Cheatham, T. E. Quantum Mechanically Derived AMBER-Compatible Heme Parameters for Various States of the Cytochrome P450 Catalytic Cycle. *J. Comput. Chem.* **2012,** 33, 119-133.
18. Wang, J.; Wolf, R. M.; Caldwell, J. W.; Kollman, P. A.; Case, D. A. Development and testing of a general amber force field. *J. Comput. Chem.* **2004,** 25, 1157-74.
19. Bayly, C. I.; Cieplak, P.; Cornell, W. D.; Kollman, P. A. A Well-Behaved Electrostatic Potential Based Method Using Charge Restraints for Deriving Atomic Charges - the Resp Model. *J. Phys. Chem.* **1993,** 97, 10269-10280.
20. M. J. Frisch, G. W. T., H. B. Schlegel, G. E. Scuseria, M. A. Robb, J. R. Cheeseman, G. Scalmani, V. Barone, G. A. Petersson, H. Nakatsuji, X. Li, M. Caricato, A. Marenich, J. Bloino, B. G. Janesko, R. Gomperts,

B. Mennucci, H. P. Hratchian, J. V. Ortiz, A. F. Izmaylov, J. L. Sonnenberg, D. Williams-Young, F. Ding, F. Lipparini, F. Egidi, J. Goings, B. Peng, A. Petrone, T. Henderson, D. Ranasinghe, V. G. Zakrzewski, J. Gao, N. Rega, G. Zheng, W. Liang, M. Hada, M. Ehara, K. Toyota, R. Fukuda, J. Hasegawa, M. Ishida, T. Nakajima, Y. Honda, O. Kitao, H. Nakai, T. Vreven, K. Throssell, J. A. Montgomery, Jr., J. E. Peralta, F. Ogliaro, M. Bearpark, J. J. Heyd, E. Brothers, K. N. Kudin, V. N. Staroverov, T. Keith, R. Kobayashi, J. Normand, K. Raghavachari, A. Rendell, J. C. Burant, S. S. Iyengar, J. Tomasi, M. Cossi, J. M. Millam, M. Klene, C. Adamo, R. Cammi, J. W. Ochterski, R. L. Martin, K. Morokuma, O. Farkas, J. B. Foresman, and D. J. Fox. *Gaussian 09, Revision A.02*, Gaussian, Inc.: Wallingford CT, 2016.

21. Wang, J.; Wang, W.; Kollman, P. A.; Case, D. A. Automatic atom type and bond type perception in molecular mechanical calculations. *J. Mol. Graph. Model.* **2006,** 25, 247-60.

22. Jorgensen, W. L.; Chandrasekhar, J.; Madura, J. D.; Impey, R. W.; Klein, M. L. Comparison of Simple Potential Functions for Simulating Liquid Water. *J. Chem. Phys.* **1983,** 79, 926-935.

23. Sousa da Silva, A. W.; Vranken, W. F. ACPYPE - AnteChamber PYthon Parser interfacE. *BMC Res. Notes* **2012,** 5, 367.

24. Van Der Spoel, D.; Lindahl, E.; Hess, B.; Groenhof, G.; Mark, A. E.; Berendsen, H. J. GROMACS: fast, flexible, and free. *J. Comput. Chem.* **2005,** 26, 1701-18.

25. Bussi, G.; Donadio, D.; Parrinello, M. Canonical sampling through velocity rescaling. *J. Chem. Phys.* **2007,** 126, 014101.

26. VandeVondele, J.; Krack, M.; Mohamed, F.; Parrinello, M.; Chassaing, T.; Hutter, J. QUICKSTEP: Fast and accurate density functional calculations using a mixed Gaussian and plane waves approach. *Comput. Phys. Commun.* **2005,** 167, 103-128.

27. Laino, T.; Mohamed, F.; Laio, A.; Parrinello, M. An Efficient Real Space Multigrid QM/MM Electrostatic Coupling. *J. Chem. Theory Comput.* **2005,** 1, 1176-84.

28. Laino, T.; Mohamed, F.; Laio, A.; Parrinello, M. An Efficient Linear-Scaling Electrostatic Coupling for Treating Periodic Boundary Conditions in QM/MM Simulations. *J. Chem. Theory Comput.* **2006,** 2, 1370-8.

29. Becke, A. D. Density-functional exchange-energy approximation with correct asymptotic behavior. *Phys. Rev. A* **1988,** 38, 3098-3100.

30. Lee, C.; Yang, W.; Parr, R. G. Development of the Colle-Salvetti correlation-energy formula into a functional of the electron density. *Phys. Rev. B* **1988,** 37, 785-789.

31. VandeVondele, J.; Hutter, J. Gaussian basis sets for accurate calculations on molecular systems in gas and condensed phases. *J. Chem. Phys.* **2007,** 127.

32. Goedecker, S.; Teter, M.; Hutter, J. Separable dual-space Gaussian pseudopotentials. *Phys. Rev. B* **1996,** 54, 1703-1710.

33. Hartwigsen, C.; Goedecker, S.; Hutter, J. Relativistic separable dual-space Gaussian pseudopotentials from H to Rn. *Phys. Rev. B* **1998,** 58, 3641-3662.

34. Vidossich, P.; Magistrato, A. QM/MM molecular dynamics studies of metal binding proteins. *Biomolecules* **2014,** 4, 616-45.

35. Brunk, E.; Rothlisberger, U. Mixed Quantum Mechanical/Molecular Mechanical Molecular Dynamics Simulations of Biological Systems in Ground and Electronically Excited States. *Chem. Rev.* **2015,** 115, 6217-63.

36. Spinello, A.; Pavlin, M.; Casalino, L.; Magistrato, A. A Dehydrogenase Dual Hydrogen Abstraction Mechanism Promotes Estrogen Biosynthesis: Can We Expand the Functional Annotation of the Aromatase Enzyme? *Chem. Eur. J.* **2018,** 24, 10840-10849.

37. Casalino, L.; Palermo, G.; Rothlisberger, U.; Magistrato, A. Who Activates the Nucleophile in Ribozyme Catalysis? An Answer from the Splicing Mechanism of Group II Introns. *J. Am. Chem. Soc.* **2016,** 138, 10374-7.

38. Nose, S. A Unified Formulation of the Constant Temperature Molecular-Dynamics Methods. *J. Chem. Phys.* **1984,** 81, 511-519.

39. Shaik, S.; Cohen, S.; Wang, Y.; Chen, H.; Kumar, D.; Thiel, W. P450 enzymes: their structure, reactivity, and selectivity-modeled by QM/MM calculations. *Chem. Rev.* **2010,** 110, 949-1017.

40. Daura, X.; Gademann, K.; Jaun, B.; Seebach, D.; van Gunsteren, W. F.; Mark, A. E. Peptide folding: When simulation meets experiment. *Angew. Chem. Int. Ed.* **1999,** 38, 236-240.

41. Miller, B. R., 3rd; McGee, T. D., Jr.; Swails, J. M.; Homeyer, N.; Gohlke, H.; Roitberg, A. E. MMPBSA.py: An Efficient Program for End-State Free Energy Calculations. *J. Chem. Theory Comput.* **2012,** 8, 3314-21.
42. Nguyen, H.; Roe, D. R.; Simmerling, C. Improved Generalized Born Solvent Model Parameters for Protein Simulations. *J. Chem. Theory Comput.* **2013,** 9, 2020-2034.
43. Humphrey, W.; Dalke, A.; Schulten, K. VMD: Visual molecular dynamics. *J. Mol. Graph. Model.* **1996,** 14, 33-38.